American Mineralogist, Volume 92, pages 1446–1455, 2007

Elastic behavior and pressure-induced structural evolution of nepheline: Implications for the nature of the modulated superstructure

G. Diego Gatta[1,*] and Ross J. Angel[2]

[1]Dipartimento di Scienze della Terra, Università degli Studi di Milano, Via Botticelli 23, I-20133 Milano, Italy
[2]Crystallography Laboratory, Department of Geosciences, Virginia Tech, Blacksburg, Virginia 24060, U.S.A.

Abstract

The elastic behavior and the pressure-induced structural evolution of a natural nepheline ($K_{0.54}Na_{3.24}Ca_{0.03}Al_4Si_4O_{16}$) were investigated by in-situ single-crystal X-ray diffraction up to 7.5 GPa with a diamond anvil cell under hydrostatic conditions. As observed in previous studies, at room conditions the diffraction pattern of nepheline includes satellite reflections, whereas the structure refinement to the Bragg reflections confirms that the O1 site is displaced from the triad at (2/3, 1/3, *z*). The reflection conditions confirm that the space group of the average structure of nepheline remains as $P6_3$ throughout the pressure range investigated, and no significant compression of the T-O bonds was measured up to 7.5 GPa. As pressure was increased to around 1 GPa the integrated intensities of the satellites decreased slightly, and at 1.8 GPa no significant intensity of the satellites was detected. Over the same pressure range the O1 site moved toward the triad and thus the tilts of the T1 and T2 tetrahedra decreased. The presence of the subsidiary non-Bragg reflections is therefore related to the split of the O1 site. When the satellites disappear at pressures above 2 GPa, the O1 site is on the triad at (2/3, 1/3, *z*), corresponding to a straight T1-O1-T2 bond. Below 2 GPa the structure responds to increased pressure by tilting of all four tetrahedra and above 2 GPa by tilting of the T3 and T4 tetrahedra alone. The change in compression mechanism arising from the changes in the O1 position is associated with changes in the compression of the unit-cell axes and the unit-cell volume. The volume can be described by fourth-order Birch-Murnaghan equation-of-state with parameters V_0 = 723.57(4) Å^3, K_{T0} = 47.32(26) GPa, K' = 2.77(24), and K'' = 0.758(79) GPa^{-1}. The elastic behavior along the **a**- and **c**-axis can be described with a "linearized" fourth-order Birch-Murnaghan equations-of-state, with the following refined parameters: a_0 = 9.9911(2) Å, $K_{T0}(a)$ = 43.1(3) GPa, $K'(a)$ = 2.5(3), and $K''(a)$ = 0.68(8) GPa^{-1} for the **a**-axis and c_0 = 8.3700(1) Å, $K_{T0}(c)$ = 58.6(3) GPa, $K'(c)$ = 4.0(3), and $K''(c)$ = 0.85(11) GPa^{-1} for the **c**-axis. The pressure-induced structural evolution in nepheline up to 7.5 GPa appears to be completely reversible. The recovery of the modulation upon complete pressure release points to the framework of nepheline having an instability corresponding to a rigid-unit mode with a wave vector corresponding to the observed positions of the satellite reflections.

Keywords: Crystal structure, nepheline, modulated structure, XRD data, single crystal, high pressure, compressibility, structural evolution

Introduction

Nepheline is a feldspathoid, with ideal formula $KNa_3Al_4Si_4O_{16}$, and occurs in a wide variety of rocks including phonolites, aplites, nepheline-pegmatites, and potassic lavas (Tilley 1954; McConnell 1962; Simmons and Peacor 1972; Merlino 1984; Tait et al. 2003). The crystal structure of nepheline was first solved by Hahn and Buerger (1955) by means of single-crystal X-ray diffraction, in space group $P6_3$. Nepheline has a tetrahedral framework structure that can be considered as a stuffed derivative of that of tridymite. The Si/Al-framework of nepheline consists of 6-membered rings parallel to (001): one-quarter are nearly hexagonal regular rings (hereafter 6mR[001]-1), whereas the other three-quarters are flattened hexagonal rings (hereafter 6mR[001]-2). The 6mR[001]-1 and 6mR[001]-2 rings form two systems of channels running parallel to [001] (Fig. 1a). The (001)-layers of tetrahedra formed by the 6mR rings are stacked along [001] to build up a 3-dimensional framework (Fig. 1b). Viewing the nepheline framework perpendicular to [001], the linkage of the tetrahedra along the **c**-axis gives rise to a complex system of adjacent 6mRs, with four different configurations, hereafter called 6mR⊥[001]-1 (Fig. 1c), 6mR⊥[001]-2 (Fig. 1d), 6mR⊥[001]-3 (Fig. 1e), 6mR⊥[001]-4 (Fig. 1f). However, the 6mRs perpendicular to [001] do not form any system of channels. The Si/Al-distribution within the tetrahedral framework of nepheline appears to be highly ordered (Sahama 1962; Dollase and Peacor 1971; Dollase and Thomas 1978; Gregorkiewitz 1984; Stebbins et al. 1986) and a recent study (Tait et al. 2003) suggests that the degree of Si/Al-order is independent of the temperature of formation. The extra-framework content in the nepheline structure is represented by two independent sites, here labeled as "K" and "Na," which lie in the 6mR[001]-1 and

* E-mail: diego.gatta@unimi.it

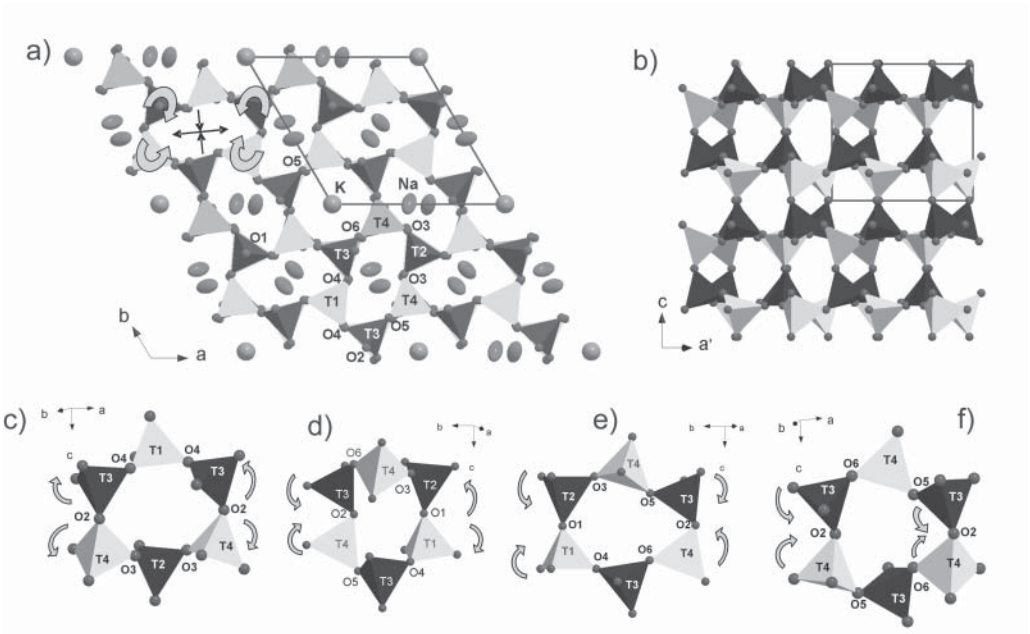

FIGURE 1. Crystal structure of nepheline viewed (**a**) down [001] and (**b**) down [010]. The extra-framework content is shown only in **a**. Thermal displacement parameters are drawn at the 50% probability level. Si-tetrahedra are represented in black, and Al-tetrahedra in gray. The four different 6-membered rings perpendicular to [001]: (**c**) 6mR⊥[001]-1, (**d**) 6mR⊥[001]-2, (**e**) 6mR⊥[001]-3, (**f**) 6mR⊥[001]-4 (see text). The directions of the tetrahedral tilts induced by increasing pressure are indicated by arrows.

6mR[001]-2 channels, respectively. In natural nephelines, the K site (Fig. 1a) is ~60% occupied by potassium with ~20–25% sodium or calcium which leaves about 1/5 of the sites vacant. The coordination number of the K site is 9. The Na site is usually fully occupied by sodium (and minor calcium) and lies in the 6mR[001]-2 channels (Fig. 1a).

Previous studies of nepheline with both single-crystal X-ray and electron-diffraction techniques (Sahama 1958; McConnell 1962, 1981) found additional non-Bragg reflections with respect to the Hahn and Buerger (1955) unit cell (with $a \sim 9.99$ Å and $c \sim 8.37$ Å). The positions of these subsidiary reflections can be defined in reciprocal space in terms of the normal reciprocal unit cell for nepheline of Hahn and Buerger (1955) by coordinates $\pm(1/3, 1/3, \pm z^*)$, with $z^* \sim 0.2$. The exact value of z^* varies with the composition of the nepheline (McConnell 1962) and is irrational. The positions of these reflections thus indicate the presence of ordering within the structure on a pattern with a threefold supercell in the (001) plane (i.e., a supercell with parameters $a\sqrt{3}$ and $b\sqrt{3}$) and an approximately fivefold supercell along [001]. There is no unique explanation concerning the nature of the ordering and modulation that gives rise to these satellite reflections. They have been variously interpreted as: (1) the result of K-vacancy ordering in the 6mR[001]-1 channels (Foreman and Peacor 1970; McConnell 1981; Merlino 1984); (2) due to domains involving different Si/Al-ordering (McConnell 1962); or (3) due to a modulation of the framework of essentially rigid tetrahedra (Parker and McConnell 1971; Parker 1972; Hayward et al. 2000). Single-crystal structure determinations provide no evidence of Al/Si disorder, so the possibility of domains of different Al/Si ordering patterns can be excluded. Recent experimental evidence points to the remaining two factors both playing a role in the development of a modulated structure and hence the satellite reflections.

The published structural data show, in fact, that the O1 site (which acts as bridge between the T1 and T2 tetrahedra (Fig. 1d) is displaced off the threefold axis at room conditions to accommodate tilting of the T1 and T2 tetrahedral and thus reduces the T1-O1-T2 bond angle from 180°. This also reduces the distance from O1 to one of the three adjacent Na sites and thus increases the formal coordination of 1/3 of these Na sites from 7 to 8 (Tait et al. 2003). The O1 position remains displaced from the triad axis up to 900 °C, even in the presence of the development of some Al/Si disorder (Foreman and Peacor 1970), while the intensity of the satellite reflections was observed to decrease with temperature but remain detectable to at least 600 °C. A further study of the time-temperature evolution of the intensities of the satellite reflections of nepheline was performed by McConnell (1981) by means of in-situ single-crystal X-ray diffraction up to 150 °C. He suggested that the strong decrease of satellite intensity during the heating experiments is the result of two different structural processes: (1) a displacive change in the tetrahedral framework, represented by the spontaneous and reversible change in satellite intensity with T; and (2) the migration of the extra-framework sites in the 6mR[001]-1 channels to produce partial disorder of the K and vacancies, which would be a kinetically hindered and irreversible process leading to the measured irreversible decrease in satellite intensities. A "Rigid Unit Mode" analysis of the framework (Hayward et al. 2000) confirmed this idea by showing that the satellite positions correspond to the wave vector of a soft mode of the framework and thus the modulation and the satellite reflections are essentially determined by the framework topology. In addition, in situ high temperature X-ray diffraction and hard mode IR-spectroscopy studies (Hayward et al. 2000) showed that the intensity of the satellite reflections sharply decreases at 308 K for (K,vacancy)-disordered nepheline and at 452 K for

(K,vacancy)-ordered nepheline, so the detailed behavior of the framework modulation is moderated by the distribution of the extra-framework cations.

The aim of this study was to investigate the high-pressure behavior of (K,vacancy)-ordered nepheline under hydrostatic conditions by means of in situ single-crystal X-ray diffraction with a diamond anvil cell, to describe the elastic behavior of nepheline and to determine whether the pressure-induced changes in the structure are consistent with the view that the essential component of the modulation is the deformation of the tetrahedral framework by a rigid-unit mode.

Experimental methods

The nepheline specimen investigated in this study, with composition ($K_{0.54}Na_{3.24}Ca_{0.03}Al_4Si_4O_{16}$), comes from the intrusive aplite of Snipe River, Tambani, Nyasaland-Malawi (no. 65984 of the Harker collection at the University of Cambridge, U.K.). The sample and the chemical analysis were kindly provided by M. Carpenter. X-ray and electron-diffraction measurements (McConnell 1962, 1981) of crystals from the same sample showed that it has the sharpest and strongest satellite reflections of any nepheline studied.

A single crystal ($220 \times 110 \times 50$ μm^3) of nepheline, optically free of defects, was used for the diffraction experiments. Accurate unit-cell constants were first measured with the crystal in air (Table 1) with a Huber four-circle diffractometer (non-monochromatized Mo$K\alpha$ radiation) using eight-position centering of 26 Bragg reflections, following the procedure of King and Finger (1979) (Table 1). Centering and vector-least-squares refinement of the unit-cell constants were performed by the SINGLE04 software according to the protocols of Ralph and Finger (1982) and Angel et al. (2000). The lattice was found to be metrically hexagonal, with unit-cell constants: $a = 9.9915(4)$ Å, $c = 8.3692(4)$ Å, and $V = 723.56(7)$ Å^3. Intensity data for the structure refinement were then collected on an Xcalibur-2 Oxford Diffraction diffractometer equipped with a Sapphire-3 CCD (Kappa-geometry, graphite-monochromatized Mo$K\alpha$ radiation). Details of the data collection procedure are reported in Table 2. The reflection absences were consistent with space group $P6_3$. Intensity data were then corrected for Lorentz-polarization and absorption effects with the CrysAlis software provided by Oxford Diffraction (2005). The same classes of satellite reflections previously reported from the same nepheline sample by McConnell (1962, 1981) were observed even in this study. The refinement of the average structure was performed with anisotropic displacement parameters using the SHELX-97 software (Sheldrick 1997), starting from the atomic coordinates of Foreman and Peacor (1970). Neutral atomic scattering factors of K, Na, Al, Si, and O from the *International Tables for Crystallography* (Wilson and Prince 1999) were used. The refinement showed the threefold degeneracy of the oxygen O1; therefore the O1 site was refined as disordered off the threefold axis. The scattering curve of the partially occupied K-site was fixed on the basis of the chemical analysis (57% by K and 24% by Na). No peak larger than ±0.68 e^-/Å^3 was present in the final difference Fourier synthesis at the end of the refinement. Details of the structural refinement are reported in Tables 2–3. The tetrahedral bond distances are indicative of essentially complete Si/Al-ordering (Table 4).

An ETH-type diamond anvil cell (DAC, Miletich et al. 2000) was used for the high-pressure experiments. Steel T301 foil, 250 μm thick, was used as gasket. The gasket foil was pre-indented to a thickness of about 120 μm before drilling a hole (~350 μm) by spark-erosion. The same crystal of nepheline previously studied at ambient conditions was cut to $140 \times 110 \times 50$ μm^3 and was placed into the gasket hole together with some ruby chips and a single-crystal of quartz used for pressure measurement (Angel et al. 1997). A methanol:ethanol (4:1) mixture was used as hydrostatic pressure-transmitting medium (Angel et al 2007). Accurate unit-cell parameters were determined at pressures ranging between 0.0001 and 7.462(7) GPa (Table 1) using 18 Bragg reflections and the same centering procedure used for the crystal in air. Five data collections at 0.0001 GPa (with crystal in DAC without any pressure medium), 1.967(5), 4.130(5), 6.108(6), and 7.462(7) GPa (Table 2) were performed with an Xcalibur-1 Oxford Diffraction diffractometer equipped with a point-detector (Kappa-geometry, graphite-monochromatized Mo$K\alpha$ radiation). No reflections that violate the conditions of $P6_3$ symmetry were observed at any pressure. Integrated intensity data (Angel 2003a, 2003b) were corrected for Lp and absorption effects due to the crystal and the DAC using the ABSORB5.2 computer program (Burnham 1966; Angel 2002). The structure refinements were conducted with the occupancy of the K-site fixed to the value adopted with the crystal in air. Because of the limited data resolution, geometrical soft restraints were used to restrain the T-O bond distances of the tetrahedra to the distances in the room-pressure crystal structure refined to the data set collected in air: the distances T1-O_n and T4-O_n were restrained to a target value of 1.71 Å with an estimated standard deviation of ±0.015 Å and the T2-O_n and T3-O_n distances were restrained to 1.61 ± 0.015 Å. Anisotropic displacement parameters were refined only for the extra-framework sites. Refined atomic positions, displacement parameters and bond distances of nepheline are summarized in Tables 3 and 4. Observed and calculated structure factors for all the structural refinements are deposited (Table 5[1]). The structural refinement based on the data collection performed with the crystal in air after the high-pressure experiment showed that the pressure-induced structural evolution up to 7.5 GPa is completely reversible, as confirmed by the refined average structure (Tables 3 and 4) and by the re-appearance of the satellite reflections.

The evolution of the satellite peaks with pressure was followed in a second loading of the same crystal with quartz into the DAC. At room pressure and at each of eight pressures up to a maximum of 1.800(5) GPa (Table 1) the orientation matrix was determined on an Xcalibur-2 diffractometer equipped with a Sapphire-3 CCD from the positions of typically 300–500 peak positions harvested from two perpendicular scans that covered most of the accessible portion reciprocal space. The strongest satellite reflections occur at $l \sim 5.8$ close to the 006 diffraction peak (McConnell 1962, 1981). The region around the 006 diffraction peak was therefore scanned at each pressure with exposures of 60 seconds per frame of 0.2° in omega. From these scans and the orientation matrix, the reciprocal lattice section at $l = 5.8$ was reconstructed and examined for the presence of the satellites. At each of these pressures in this second loading, the unit-cell parameters of both nepheline and quartz were also determined on the Huber diffractometer (Table 1). Three further measurements of unit-cell parameters were also made up to 3.7 GPa, without accompanying CCD measurements (Table 1).

Table 1. Unit-cell parameters of nepheline at pressure

P (GPa)	*a* (Å)	*c* (Å)	*V* (Å^3)
First loading			
0.0001	9.9915(4)	8.3692(4)	723.56(7)
0.0001*	9.9910(3)	8.3702(2)	723.58(4)
0.464(4)	9.9570(4)	8.3486(3)	716.80(7)
1.206(4)	9.9029(4)	8.3159(3)	706.27(5)
1.967(5)	9.8499(2)	8.2838(2)	696.03(4)
3.330(4)	9.7629(2)	8.2311(2)	679.44(3)
3.759(9)	9.7384(3)	8.2158(2)	674.78(5)
4.130(5)	9.7178(2)	8.2030(2)	670.87(3)
4.927(4)	9.6760(2)	8.1774(2)	663.04(3)
6.108(6)	9.6189(2)	8.1423(2)	652.43(3)
6.640(4)	9.5940(2)	8.1272(2)	647.84(3)
7.462(7)	9.5587(3)	8.1051(2)	641.34(4)
0.0001†	9.9907(2)	8.3695(2)	723.47(4)
Second loading			
0.0001*	9.9910(2)	8.3700(1)	723.56(4)
0.105(6)	9.9822(3)	8.3649(2)	721.85(5)
0.272(6)	9.9696(3)	8.3571(1)	719.36(4)
0.511(4)	9.9522(3)	8.3461(2)	715.89(4)
0.800(5)	9.9308(2)	8.3330(1)	711.70(4)
0.938(5)	9.9205(2)	8.3267(1)	709.69(3)
1.074(5)	9.9116(3)	8.3210(2)	707.93(4)
1.423(5)	9.8862(2)	8.3059(2)	703.03(4)
1.800(5)	9.8605(2)	8.2900(1)	698.05(3)
2.293(6)	9.8273(2)	8.2700(1)	691.68(4)
2.886(6)	9.7899(2)	8.2474(1)	684.54(3)
3.672(5)	9.7434(3)	8.2188(2)	675.70(5)

Note: Estimated standard deviations in the last digit are in parentheses.
* Crystal in the DAC without *P*-medium.
† Crystal in the DAC without *P*-medium after decompression.

[1] Deposit item AM-07-026, Table 5 (observed and calculated structure factors for all the structural refinements). Deposit items are available two ways: For a paper copy contact the Business Office of the Mineralogical Society of America (see inside front cover of recent issue) for price information. For an electronic copy visit the MSA web site at http://www.minsocam.org, go to the American Mineralogist Contents, find the table of contents for the specific volume/issue wanted, and then click on the deposit link there.

TABLE 2. Details of data collection and refinements of nepheline at different pressures

Pressure (GPa)	0.0001	0.0001*	1.967	4.130	6.108	7.462	0.0001†
Crystal size (μm)	220 × 110 × 50	140 × 110 × 50	140 × 110 × 50	140 × 110 × 50	140 × 110 × 50	140 × 110 × 50	140 × 110 × 50
a (Å)	9.9995(5)	9.9910(3)	9.8499(3)	9.7178(2)	9.6189(2)	9.5587(3)	9.9907(2)
c (Å)	8.3766(6)	8.3702(2)	8.2838(2)	8.2030(2)	8.1423(2)	8.1051(2)	8.3695(2)
Space Group	$P6_3$	$P6_3$	$P6_3$	$P6_3$	$P6_3$	$P6_3$	$P6_3$
Radiation	Mo*K*α	Mo*K*α	Mo*K*α	Mo*K*α	Mo*K*α	Mo*K*α	Mo*K*α
Detector type	CCD	Point det.	Point det.	Point det.	Point det.	Point det.	CCD
Max 2θ(°)	60.14	69.56	69.87	69.97	69.54	69.93	60.09
Scan type	ω/ϕ	ω	ω	ω	ω	ω	ω/ϕ
Scan speed (°/s)	–	0.05	0.05	0.05	0.05	0.05	–
Scan width (°)	1.0°/frame	1.2	1.2	1.2	1.2	1.2	1.0°/frame
CCD frame processed	942	–	–	–	–	–	474
Exposure (s/frame)	5	–	–	–	–	–	10
Reflections measured	14772	505	662	635	651	612	7639
Unique refl. (total)	1418	401	472	456	470	410	1394
Unique refl. with $F_o > 4\sigma(F_o)$	1374	361	431	428	441	376	991
Parameters refined	91	50	50	48	48	48	91
R_{int}	0.0465	0.0376	0.0455	0.0446	0.0368	0.0578	0.0376
R_1	0.0334	0.0581	0.0488	0.0422	0.0440	0.0458	0.0291
wR_2	0.0996	0.1336	0.1051	0.0936	0.1054	0.1052	0.0829

Notes: Estimated standard deviations are in parentheses.
$R_{int} = \Sigma|F^2_{obs} - F^2_{obs}(mean)|/\Sigma(F^2_{obs})$; $R_1 = \Sigma(||F_{obs}| - |F_{calc}||)/\Sigma|F_{obs}|$; $wR_2 = \{\Sigma[w(F^2_{obs} - F^2_{calc})^2]/\Sigma[w(F^2_{obs})^2]\}^{0.5}$, $w = 1/[\sigma^2(F^2_{obs}) + (a \cdot P)^2 + b \cdot P]$, $P = [\text{Max}(F^2_{obs}, 0) + 2 \cdot F^2_{calc}]/3$.
* Crystal in the DAC without *P*-medium.
† Crystal in the DAC without *P*-medium after decompression.

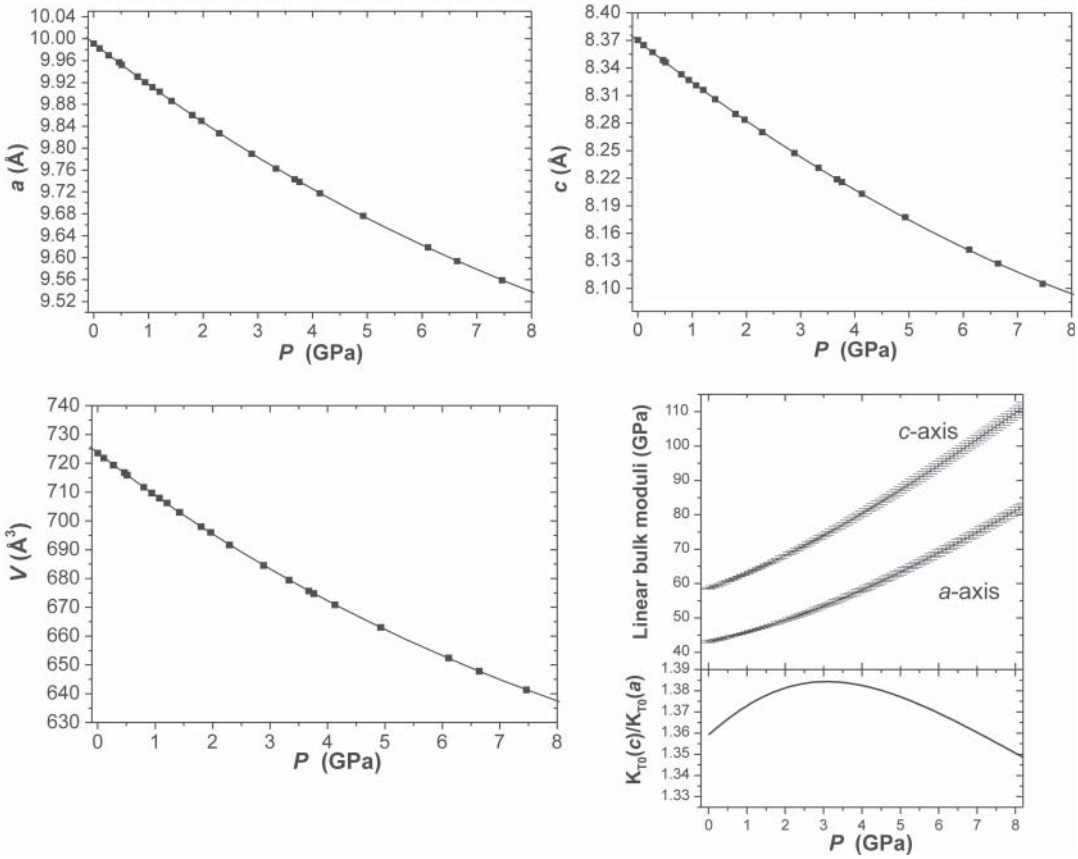

FIGURE 2. Variation of the unit-cell parameters of nepheline with pressure and evolution of the calculated linear bulk moduli, $K_{T0}(a)$ and $K_{T0}(c)$, with *P*. For the experimental data, the solid lines represent the axial and volume fourth-order Birch-Murnaghan EoS fits. The e.s.d. values are slightly smaller than the size of the symbols.

RESULTS

Elastic behavior

The evolution of the unit-cell parameters of nepheline at high pressure is shown in Figure 2. Axial and volume Eulerian finite strains $\{f_e = [(V_0/V)^{2/3} - 1]/2\}$ vs. normalized stress $\{F_e = P/[3f(1 + 2f)^{5/2}]$, Angel 2000$\}$ were calculated using the a_0, c_0, and V_0 values measured with the crystal in the DAC. The resulting f_e-F_e plots (Fig. 3) exhibit clearly different slopes below and above

TABLE 3. Refined atomic positions and thermal displacement parameters (Å²) of nepheline at different pressures

Sites	*x*	*y*	*z*	U_{iso}*, U_{eq}†	Sites	*x*	*y*	*z*	U_{iso}*, U_{eq}†
K	0	0	0.00410(42)	0.03296(29)†	O1	0.6619(24)	0.2891(12)	0.50178(83)	0.0335(14)†
(2*a*)	0	0	0.0051(28)	0.032(17)†	(6*c*, 2*b*)	0.6565(46)	0.2857(26)	0.5022(18)	0.0234(59)*
	0	0	0.0029(18)	0.0268(10)†		0.6621(39)	0.2962(22)	0.5011(17)	0.0238(48)*
	0	0	0.0041(17)	0.0190(8)†		2/3	1/3	0.5059(14)	0.0406(27)*
	0	0	–0.0073(14)	0.0171(9)†		2/3	1/3	0.4957(15)	0.0355(25)*
	0	0	0.0028(20)	0.0220(11)†		2/3	1/3	0.5018(15)	0.0299(27)*
	0	0	0.00350(81)	0.03448(37)†		0.6708(45)	0.2957(35)	0.5008(11)	0.0348(32)†
Na	0.55412(10)	0.99724(10)	0.50845(32)	0 .02537(21)†	O2	0.97288(20)	0.68347(25)	0.00309(41)	0.03350(40)†
(2*a*)	0.55384(60)	0.99711(67)	0.5071(17)	0.0239(13)†	(6*c*)	0.9740(11)	0.6844(11)	0.0021(14)	0.0244(19)*
	0.55578(41)	0.99782(43)	0.5066(14)	0.0217(8)†		0.98771(68)	0.69126(68)	0.0055(13)	0.0205(12)*
	0.55760(34)	0.99930(37)	0.5064(12)	0.0182(7)†		1.00071(57)	0.69849(56)	0.0042(12)	0.0144(9)*
	0.55850(35)	1.00022(37)	0.5027(13)	0.0169(6)†		1.00916(58)	0.70138(59)	–0.0036(12)	0.0138(9)*
	0.56008(41)	1.00140(46)	0.5064(14)	0.0195(8)†		1.01431(70)	0.70341(69)	0.0017(12)	0.0143(12)*
	0.55414(11)	0.99762(11)	0.50785(55)	0.02594(24)†		0.97316(24)	0.68409(28)	0.00228(64)	0.03106(49)†
T1	2/3	1/3	0.70194(17)	0.01271(28)†	O3	0.82649(29)	0.47750(28)	0.25170(59)	0.03807(72)†
(2*b*)	2/3	1/3	0.7028(12)	0.0069(18)*	(6*c*)	0.8220(18)	0.4743(13)	0.2304(18)	0.0373(40)*
	2/3	1/3	0.7049(11)	0.0096(16)*		0.8293(11)	0.47474(90)	0.2310(12)	0.0222(21)*
	2/3	1/3	0.71222(76)	0.0087(16)*		0.8336(11)	0.47374(90)	0.2310(10)	0.0207(20)*
	2/3	1/3	0.70282(87)	0.0085(16)*		0.8360(11)	0.47420(92)	0.2237(11)	0.0172(21)*
	2/3	1/3	0.71012(96)	0.0108(19)*		0.8408(15)	0.4758(12)	0.2446(15)	0.0202(32)*
	2/3	1/3	0.70209(33)	0.01355(56)†		0.82600(49)	0.47725(41)	0.25143(87)	0.0360(11)†
T2	2/3	1/3	0.31362(17)	0.01423(26)†	O4	0.83665(30)	0.48973(29)	0.76444(56)	0.03390(60)†
(2*b*)	2/3	1/3	0.3144(14)	0.0173(23)*	(6*c*)	0.8393(13)	0.4905(12)	0.7526(14)	0.0198(28)*
	2/3	1/3	0.3107(10)	0.0113(16)*		0.8432(11)	0.48988(94)	0.7551(12)	0.0244(25)*
	2/3	1/3	0.31158(74)	0.0075(13)*		0.8456(10)	0.48771(89)	0.7642(10)	0.0166(18)*
	2/3	1/3	0.29904(78)	0.0089(15)*		0.8486(11)	0.48610(95)	0.7632(11)	0.0175(22)*
	2/3	1/3	0.30483(83)	0.0101(17)*		0.8457(14)	0.4826(12)	0.7859(14)	0.0164(29)*
	2/3	1/3	0.31353(29)	0.01392(52)†		0.83662(45)	0.48965(40)	0.76565(86)	0.0328(10)†
T3	0.90568(8)	0.66614(8)	0.82276(8)	0.01378(21)†	O5	0.77365(26)	0.71475(27)	0.82462(39)	0.02064(45)†
(6*c*)	0.90486(69)	0.66596(71)	0.82172(40)	0.0112(10)*	(6*c*)	0.7705(13)	0.7130(13)	0.8226(13)	0.0108(22)*
	0.91197(47)	0.66799(47)	0.82507(31)	0.0092(8)*		0.77506(98)	0.71427(98)	0.8302(11)	0.0138(19)*
	0.91817(48)	0.67174(51)	0.82475(24)	0.0091(8)*		0.77691(92)	0.71442(92)	0.8345(10)	0.0126(19)*
	0.92093(46)	0.67173(45)	0.81891(24)	0.0081(8)*		0.77757(86)	0.71312(94)	0.8327(9)	0.0107(16)*
	0.92358(62)	0.67276(69)	0.82528(33)	0.0100(10)*		0.7801(10)	0.7144(11)	0.8417(9)	0.0077(17)*
	0.90606(16)	0.66644(16)	0.82291(11)	0.01334(30)†		0.77305(48)	0.71396(42)	0.82379(67)	0.01929(78)†
T4	0.90645(9)	0.66759(9)	0.19630(9)	0.01235(22)†	O6	0.77607(26)	0.73287(26)	0.20149(41)	0.02315(48)†
(6*c*)	0.90743(76)	0.66818(84)	0.19535(49)	0.0128(13)*	(6*c*)	0.7787(17)	0.7369(17)	0.2016(17)	0.0274(39)*
	0.91316(55)	0.67064(55)	0.19626(37)	0.0114(10)*		0.7815(11)	0.7375(12)	0.1941(12)	0.0212(26)*
	0.91775(51)	0.67115(56)	0.19370(27)	0.0075(8)*		0.7850(10)	0.7392(10)	0.1875(10)	0.0135(20)*
	0.92279(51)	0.67442(49)	0.18671(28)	0.0073(9)*		0.7868(9)	0.7399(10)	0.1798(10)	0.0135(19)*
	0.92423(69)	0.67448(80)	0.19201(40)	0.0114(13)*		0.7866(12)	0.7396(13)	0.1862(12)	0.0197(25)*
	0.90620(18)	0.66767(18)	0.19635(14)	0.01306(34)†		0.77664(47)	0.73391(42)	0.20013(72)	0.0230(9)†

Notes: Estimated standard deviations are in parentheses. For each site, the values from top to bottom correspond to the refinement at 0.0001 (in air), 0.0001 (with crystal in the DAC), 1.967(5), 4.130(5), 6.108(6), 7.462(7), and 0.0001 GPa (with crystal in air, after decompression). The refinements with the crystal in air have been performed with all the atoms anisotropic, whereas all the refinements with the crystal in the DAC have been performed considering the K and Na sites as anisotropic and all the other sites as isotropic. U_{eq} (†) for the anisotropic atoms and U_{iso} (*) for the isotropic atoms are given. For the K site, a scattering curve based on a partial occupancy with 57%K + 24%Na (see text) was used. T1 and T4 sites are fully occupied by Al, whereas T2 and T3 are occupied by Si. Below 2 GPa, the O1 site is disordered off the threefold axis with formal occupancy of 1/3.

a pressure of ~2 GPa. Since the f_e-F_e plot can be strongly influenced by the uncertainty in V_0 (or a_0^3 or c_0^3, Angel 2000; Angel and Jackson 2002), we confirmed that the changes in slopes are present whether the a_0, c_0, V_0 values used to calculate f_e and F_e are taken from the measurement of the crystal in air (before the high-pressure experiment) or from that of the crystal in the DAC at P = 0.0001 GPa (without any P-medium) after the high-pressure experiment. Therefore, the elastic behavior of nepheline at high pressure should be described as two separate parts or with a fourth-order isothermal Equation-of-State.

The P-V data were fitted with a fourth-order Birch-Murnaghan Equation-of-State (IV-BM-EoS) (Birch 1947), with the EOS-FIT5.2 computer program (Angel 2001). The elastic parameters obtained, using the data weighted by the uncertainties in P-V, are the following: V_0 = 723.57(4) Å³, K_{T0} = 47.32(26) GPa, K' = 2.77(24), and K'' = 0.758(79) GPa^{-1} (Fig. 2). The adiabatic bulk modulus obtained by Bonczar and Barsch (1975) by in situ single-crystal ultrasonic measurements [$B_0 = 4.9(7) \times 10^{11}$ dyn/cm² ≈ 49(7) GPa] is consistent with the value obtained in the current study. The elastic behavior along the **a** and **c** axis can be described with a "linearized" IV-BM-EoS (Angel 2000). The refined parameters of the linearized EoS are: a_0 = 9.9911(2) Å, $K_{T0}(a)$ = 43.1(3) GPa, $K'(a)$ = 2.5(3), and $K''(a)$ = 0.68(8) GPa^{-1} for the **a**-axis and c_0 = 8.3700(1) Å, $K_{T0}(c)$ = 58.6(3) GPa, $K'(c)$ = 4.0(3) and $K''(c)$ = 0.85(11) GPa^{-1} for the **c**-axis (Fig. 2). The elastic anisotropy of nepheline is almost constant with pressure, being $K_{T0}(c)$:$K_{T0}(a)$ = 1.365 ± 0.015 within the P-range investigated (Fig. 2).

Satellite intensities

At room pressure in the DAC all six of the satellites are immediately visible in the reciprocal lattice section l = 5.8 reconstructed from long-exposure CCD scans of the second loading of the sample, even though their peak intensity is only some 400 counts above a background of typically 2000 counts. The integrated intensities of the individual satellites obtained from this section are between 1.5–2.0 times their estimated standard deviations obtained from counting statistics including the effect

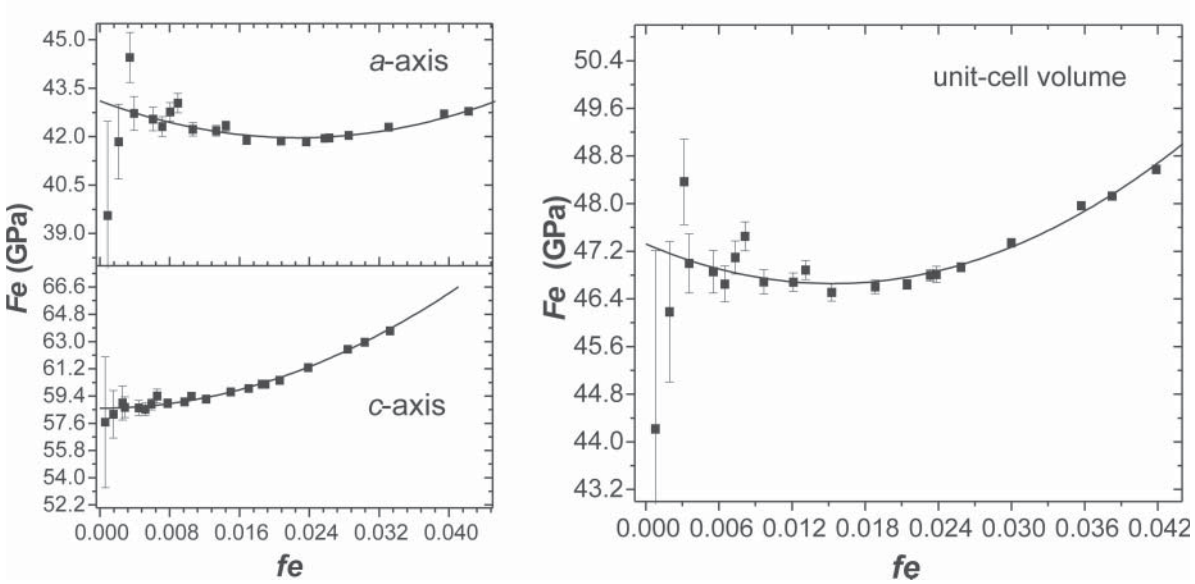

FIGURE 3. Axial and volume Eulerian finite strain vs. normalized stress (f_e-F_e plot) for nepheline; e.s.d. values calculated according to Heinz and Jeanloz (1984) and Angel (2000) and include the measured uncertainty in V_0. The solid lines represent the f_e-F_e evolution calculated from the refined fourth-order Birch-Murnaghan EoS (see text).

of the high backgrounds. Within the large uncertainties they are all equal in intensity. As pressure is increased to around 1 GPa, the satellites became less distinct, and their integrated intensities showed a marginal decrease (Fig. 4). In the data set collected at 1.423(5) GPa only two of the satellite positions show any sign of significant intensity, and the integrated intensities of these two positions are 1.2 and 1.6 e.s.d. values. No significant intensity was detected at 1.800(5) GPa. At the pressures at which the satellites were still visible there was no indication of a shift of the satellite positions from their positions at room pressure, at least within the estimated resolution of ±0.03 in reciprocal lattice units. Neither was there any indication of broadening of the satellite reflections with pressure, nor development of the diffuse streaks that develop between the satellites after annealing nepheline at high temperatures (Boffa-Ballaran and Angel, unpublished data). These results therefore suggest that the structural modification giving rise to the satellites decreases in amplitude with increasing pressure, without either a loss in coherence or a change in the wavelength of the modulation. However, whether the modulation completely disappears above 1.8 GPa or whether it survives in a weaker form cannot be determined from the measurement of the intensities alone.

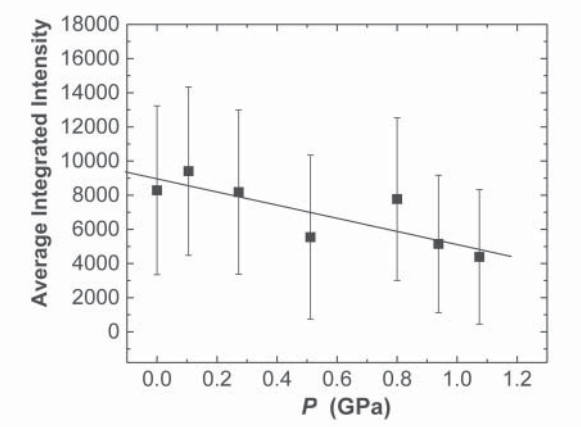

FIGURE 4. Variation of average integrated satellite intensities visible in the reciprocal lattice section l = 5.8 with pressure. Error bars are the average e.s.d. in the intensity of the six satellites, not the population standard deviation. The solid line represents the weighted linear fit through the data.

Structural evolution with pressure

The high-pressure evolution of the crystal structure of nepheline is described here on the basis of five structural refinements at different pressures (Tables 2, 3, and 4) to the Bragg reflections alone. The refined structures at low pressures are therefore a space and time average over the real local modulated structure, and this averaging is apparent in elongated displacement ellipsoids and split sites. The refined framework and extra-framework site positions based on the data collected with the crystal in air are in good agreement with those reported in the previous studies on Si/Al-ordered nepheline (Tait et al. 2003) with the T-O bond lengths indicating essentially complete ordering of Al into T1 and T4, and Si into T2 and T3, and thus strict alternation of Si and Al throughout the tetrahedral framework (Tables 4 and 6). The structural parameters refined with the crystal in the DAC show only small differences with respect to those obtained for the crystal in air (Tables 3 and 4).

The key to understanding the evolution of the tetrahedral framework of nepheline is the O1 site that is the oxygen shared between the T1 and T2 tetrahedral sites. All three of these sites are topologically required to be located upon symmetry-equivalent positions on the threefold axis at 2/3 1/3 z, and this requires that the T1-O1-T2 linkage be linear. However, difference Fourier

TABLE 4. Bond distances (Å) of nepheline at different pressures

P (GPa)	0.0001	0.0001*	1.967	4.130	6.108	7.462	0.0001†
K-O6 (×3)	2.984(3)	2.948(20)	2.874(13)	2.785(11)	2.767(10)	2.736(14)	2.970(6)
K-O5 (×3)	3.010(3)	3.032(9)	2.939(11)	2.885(11)	2.826(10)	2.799(12)	3.015(5)
K-O2 (×3)	3.039(2)	3.040(16)	2.982(6)	2.933(5)	2.918(5)	2.906(6)	3.031(2)
Na-O5	2.484(3)	2.466(16)	2.410(11)	2.363(9)	2.332(9)	2.306(11)	2.480(5)
Na-O2	2.534(2)	2.533(11)	2.506(7)	2.489(5)	2.456(6)	2.446(7)	2.535(2)
Na-O1	2.557(8)	2.532(21)	2.581(17)	2.867(3)	2.832(3)	2.806(4)	2.600(27)
Na-O4	2.587(5)	2.500(18)	2.467(14)	2.486(12)	2.467(13)	2.480(14)	2.596(8)
Na-O6	2.588(3)	2.618(19)	2.555(12)	2.507(10)	2.474(10)	2.465(13)	2.589(5)
Na-O3	2.639(5)	2.681(18)	2.617(13)	2.566(11)	2.515(12)	2.492(16)	2.635(8)
Na-O4′	2.779(4)	2.826(17)	2.756(13)	2.655(11)	2.595(12)	2.595(16)	2.766(7)
Na-O3′	2.788(5)	2.797(20)	2.718(15)	2.662(13)	2.650(13)	2.588(15)	2.791(7)
T1-O4	1.718(3)	1.705(9)	1.701(8)	1.687(7)	1.701(8)	1.703(9)	1.718(4)
T1-O1	1.729(7) ×3	1.734(13) ×3	1.724(12) ×3	1.692(11) ×1	1.686(11) ×1	1.688(11) ×1	1.731(9) ×3
T2-O3	1.612(3)	1.643(11)	1.647(8)	1.648(7)	1.630(7)	1.611(10)	1.607(4)
T2-O1	1.631(7) ×3	1.631(13) ×3	1.615(11) ×3	1.594(11) ×1	1.601(10) ×1	1.597(11) ×1	1.617(9) ×3
T3-O4	1.615(3)	1.640(10)	1.638(8)	1.637(8)	1.623(8)	1.615(9)	1.614(4)
T3-O6	1.618(3)	1.616(11)	1.632(9)	1.629(8)	1.623(8)	1.601(9)	1.621(5)
T3-O5	1.619(2)	1.629(9)	1.626(8)	1.622(7)	1.619(7)	1.613(8)	1.619(4)
T3-O2	1.627(3)	1.632(11)	1.634(10)	1.634(9)	1.627(9)	1.621(9)	1.617(5)
T4-O3	1.717(3)	1.707(11)	1.701(8)	1.695(8)	1.699(8)	1.706(10)	1.717(4)
T4-O6	1.726(2)	1.735(11)	1.723(9)	1.719(8)	1.713(8)	1.715(9)	1.724(4)
T4-O2	1.726(3)	1.726(11)	1.711(10)	1.709(9)	1.716(9)	1.720(9)	1.733(5)
T4-O5	1.728(3)	1.701(10)	1.705(9)	1.710(8)	1.703(8)	1.719(8)	1.724(5)

Note: Estimated standard deviations are in parentheses.
* Crystal in the DAC without *P*-medium.
† Crystal in air after decompression

maps (Fig. 5) calculated from the structure factors collected at room pressure and phases from a model of the average structure without the O1 site clearly show that the O1 position is split off the threefold axis to $x \sim 0.656$ and $y \sim 0.286$. Within the unit cell of the average structure there are three symmetry-equivalent positions for the O1 site around the triad axis (Fig. 5, Tables 3 and 4), and each therefore has a formal occupancy of 1/3. The shift of the O1 atom off the triad axis allows the T1-O1-T2 bond angle to be reduced from 180° to ~150°. The elongation along [001] of the anisotropic displacement parameters of the O3 and O4 oxygen atoms that form the respective bases of the T1 and T2 tetrahedra indicates that the T1 and T2 tetrahedra are tilted (rather than being internally deformed) by the shift of the O1 atom off the triad axis (Dollase 1970; Tait et al. 2003).

Within the precision of the structure refinements at high pressures, we are unable to detect any significant compression of the T-O bond lengths or changes in the internal O-T-O bond angles (Table 4). Distance least-squares (DLS) simulations of the structure at 7.462 GPa with the DLS-76 program (Baerlocher et al. 1977), in which the tetrahedra were required to have idealized regular geometry for SiO_4 and AlO_4 and the O1 was fixed on the triad axis, reproduced the overall pattern of tetrahedral tilts found in the structure determined by experiment; the DLS simulation yielded T-O-T angles within 2° of the observed angles except for O2, which was under-estimated as 122° instead of the observed 125.6°. We can therefore consider the changes in the framework of nepheline at pressure to be almost completely the result of the tilting of rigid tetrahedral units.

At 1.967(5) GPa, the split of the O1 off the triad axis is still clearly indicated by the difference Fourier map (Fig. 5), whereas at 4.130(5) GPa and higher pressures the O1 site appears to lie on the threefold axis (with coordinates 2/3, 1/3, *z*) (Fig. 5, Table 3) within the resolution of our measurements. Thus the application of pressure removes the tilts of the T1 and T2 tetrahedra, increases the T1-O1-T2 angle to 180°, and places the bases of the T1 and T2 tetrahedra parallel to (001). The pattern of changes in the other T-O-T angles is also caused by this un-tilting, and the T3-O2-T4 angle decreases significantly so as to allow the compression of the [001] direction even while the parallel T1-T2 distance is increased by the un-tilting of their tetrahedra.

These changes in tilting of the tetrahedral framework give rise

TABLE 6. Selected structural parameters of nepheline at different pressure

P (GPa)	0.0001*	1.967	4.130	6.108	7.462
T2-O1-T1 (°)	150.1(13)	156.1(11)	180	180	180
T4-O2-T3 (°)	137.3(6)	133.5(4)	129.7(3)	127.2(3)	125.6(4)
T4-O3-T2(°)	140.2(11)	137.9(7)	136.7(7)	136.8(7)	136.6(10)
T1-O4-T3(°)	138.6(9)	138.1(7)	137.5(6)	136.1(7)	135.9(9)
T3-O5-T4(°)	140.9(9)	137.8(7)	134.6(6)	131.7(5)	130.3(6)
T3-O6-T4(°)	142.0(10)	136.4(7)	132.9(6)	132.2(6)	131.9(8)
6mR[001]-1					
O6-O5 (Å)	5.174(22)	5.091(20)	5.017(21)	4.974(22)	4.936(24)
6mR[001]-2					
O3-$O4_{long}$ (Å)	6.793(24)	6.809(21)	6.800(22)	6.791(24)	6.778(24)
O3-$O4_{short}$ (Å)	3.227(18)	3.072(18)	2.961(17)	2.880(24)	2.838(24)
O6-O5 (Å)	5.165(23)	5.171(22)	5.161(22)	5.134(24)	5.125(24)
ε	0.475	0.451	0.435	0.424	0.419
6mR⊥[001]-1					
O2-O2 (Å)	5.734(20)	5.817(21)	5.902(23)	5.930(21)	5.950(22)
O3-O4 (Å)	4.002(18)	3.945(17)	3.831(18)	3.752(19)	3.718(18)
T1-T2 (Å)	5.119(21)	5.018(20)	4.916(16)	4.855(22)	4.820(24)
T4-T4 (Å)	5.176(22)	5.158(21)	5.115(22)	5.124(23)	5.099(23)
6mR⊥[001]-2					
O2-O1 (Å)	4.111(15)	3.877(18)	3.398(16)	3.298(19)	3.239(21)
T4-T3 (Å)	5.243(18)	5.209(19)	5.176(22)	5.148(21)	5.133(20)
T4-T1 (Å)	4.263(16)	4.159(18)	4.063(21)	3.989(19)	3.951(20)
6mR⊥[001]-3					
O1-O2 (Å)	6.618(21)	6.548(23)	6.336(25)	6.340(25)	6.341(24)
O3-O4 (Å)	4.375(17)	4.344(21)	4.376(19)	4.394(21)	4.388(20)
O5-O6 (Å)	3.179(15)	3.021(17)	2.903(17)	2.836(18)	2.800(19)
T1-T4 (Å)	5.729(18)	5.692(19)	5.660(23)	5.635(22)	5.613(24)
T4-T3 (Å)	5.243(20)	5.209(22)	5.176(22)	5.148(21)	5.133(22)
6mR⊥[001]-4					
O2-O2 (Å)	5.251(23)	5.166(22)	5.081(24)	5.053(23)	5.033(23)
O6-$O5_{long}$ (Å)	5.202(19)	5.273(21)	5.312(22)	5.320(21)	5.318(24)
O6-$O5_{short}$ (Å)	3.179(16)	3.021(18)	2.903(17)	2.836(19)	2.800(18)
T3-T4 (Å)	5.243(20)	5.209(21)	5.176(22)	5.148(22)	5.133(21)
T4-T4 (Å)	5.132(23)	5.044(22)	4.989(19)	4.909(21)	4.884(20)

Note: Estimated standard deviations are in parentheses. ε = (O3-$O4_{short}$)/(O3-$O4_{long}$); σ(ε) < 0.005 at any given pressure.
* Crystal in the DAC without *P*-medium.

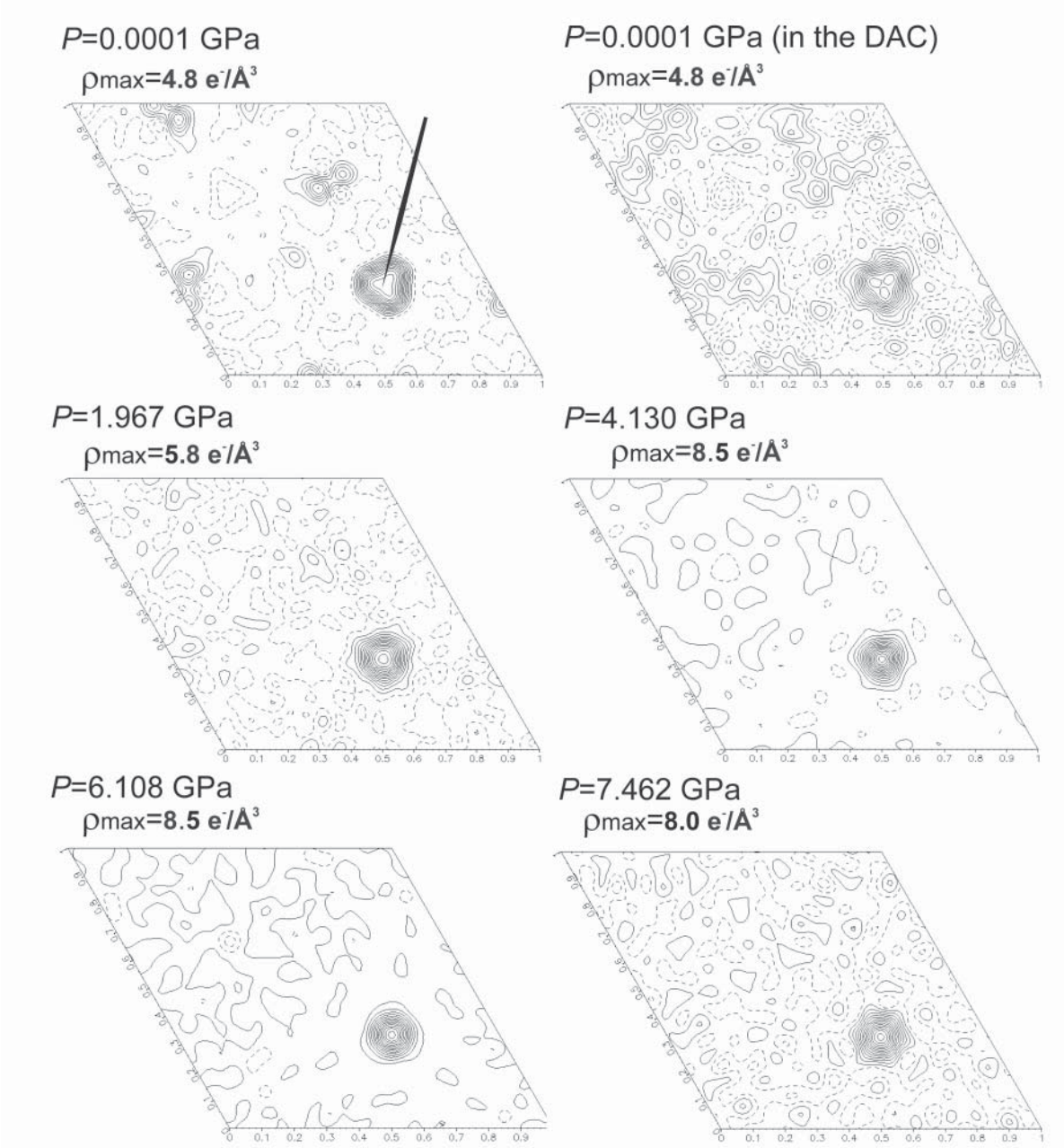

FIGURE 5. Difference Fourier maps of nepheline at $z \sim 0.508$ at different pressures calculated with coefficients F_o-F_c and phased by F_c. To avoid biasing the results in the neighborhood of the triad axis at $x = 2/3$ and $y = 1/3$, the F_c were calculated from a structural model of nepheline without the O1 site. The black arrow in the first map indicates the location of the triad axis.

to deformations of the system of channels that run along [001]. As a consequence of the decrease in all of the T-O-T angles except that at O1, the "ellipticity ratio" of the 6mR[001]-2 [here defined as $\varepsilon = (O3\text{-}O4_{short}/O3\text{-}O4_{long})$] decreases monotonically with pressure, which implies an increase in ellipticity (Table 6). The increase of the $O3\text{-}O4_{long}$ "diameter" of any given 6mR[001]-2 is balanced by the decrease of the $O3\text{-}O4_{short}$ diameter of the adjacent 6mR[001]-2 (Fig. 1a, Table 6). On the basis of this cooperative mechanism, the framework is strongly compressed on (001) despite the configuration of the nearly regular 6mR[001]-1 being maintained.

More complicated is the analysis of the pressure-induced structural effects along [001], due to the complex configuration of the four adjacent 6-membered rings perpendicular to the **c**-axis (i.e., 6mR⊥[001]-1, 6mR⊥[001]-2, 6mR⊥[001]–3, 6mR⊥[001]–4). The evolution of all the 6mRs⊥[001] is driven by the tetrahedral tilting represented by the variation with pressure of the angles T2-O1-T1, T4-O2-T3, T4-O3-T2, T1-O4-T3,

T3-O5-T4, and T3-O6-T4 (Figs. 1c, 1d, 1e, and 1f, Table 6). For the 6mR⊥[001]-1, the tetrahedral tilting at high pressure gives rise to an extension of the "diameter" O2-O2, which implies an expansion on (001) (Fig. 1c, Table 6). In contrast, the distances O3-O4 and T1-T2 of the same 6mR decrease along [001] (Fig. 1c, Table 6). The other three systems of rings show a reduction of the "diameters" parallel and perpendicular to [001]. In fact, the distances O2-O1 and T4-T1 (perpendicular to [001]) and T4-T3 (parallel to [001]) belonging to 6mR⊥[001]-2, the distances O1-O3 and T1-T4 (⊥[001]) and T3-T4 (//[001]) belonging to the 6mR⊥[001]–3 and the distances O2-O2 (⊥[001]) and T4-T3 (//[001]) belonging to 6mR⊥[001]–4 decrease with pressure (Figs. 1d, 1e, and 1f, Table 6). The expansion of the O2-O2 distance of the 6mR⊥[001]-1 on (001) is counterbalanced by the reduction of the O2-O1 distances of the 6mR⊥[001]-2 and 6mR⊥[001]–3 and O2-O2 of the 6mR⊥[001]–4.

The structure refinements show that the topological configuration of the extra-framework content is basically maintained at high pressure for the K-polyhedron with a monotonic decrease in K-O bond distances with pressure (Table 4). For the Na-polyhedron, there is a significant change in the lengths and patterns of Na-O1 bonds between the refinements of the structure at 1.967 and 4.130 GPa. At pressures below ~2 GPa the threefold degeneracy of the oxygen O1 implies a short Na-O1 bond distance to one-third of the Na atoms of about 2.55 Å. At higher pressures, the shift of the O1-site to the triad gives rise to a Na-O1 distance of about 2.87 Å to all of the Na atoms. This is the longest Na-O distance (Table 4), and it remains the longest up to the maximum pressure achieved in this experiment. This increase in the bond-length to the O1 site is clearly compensated by the reduction in the bonds from Na to O3, O4', and O3' (Table 4).

Discussion and concluding remarks

The changes in the elastic behavior of nepheline, the structural evolution and the behavior of the satellite reflections with pressure appear to be related effects. At low pressures (up to ca. 2 GPa) the structure evolves by un-tilting the T1 and T2 tetrahedra by shifting the average position of the O1 toward the triad axis so that the T1-O1-T2 angle evolves toward 180°. This is accompanied by changes in the tilts of the T3 and T4 tetrahedra. The continued presence and sharpness of the satellite reflections indicates that the true local structure maintains a well-ordered modulation of these tilts of tetrahedra that corresponds to the threefold super-cell in the (001) plane (McConnell 1962). The decrease in the intensity of the satellites is due to the decrease in the magnitude of the displacement of the O1 sites from the triad axis. This decrease in displacement can reasonably be expected to be the cause of the low initial K' of the compression within the (001) plane (i.e., the compression of [100]).

At pressures around 2 GPa, we observe the shift of the O1 site on to the triad and the simultaneous disappearance of the satellite reflections; at the same pressure we have the minimum value of the normalized stress in the volume f_e-F_e plot (Fig. 3). This point represents a slight change in the elastic behavior as a result of the change in compression mechanism due to the cessation of the tilting of the T1 and T2 tetrahedra because the O1 has reached the triad axis. The compression at higher pressures can then only be accommodated by tilting of the T3 and T4 tetrahedra alone and this reduction in framework flexibility is presumably the cause of the increased rate of stiffening of the structure (Fig. 3). Our data are insufficient to determine whether the changes in compression mechanism in nepheline at 2–3 GPa correspond to a phase transition with no symmetry change and undetectable volume change, or whether they are just a change in internal compression mechanism. In either case, the IV-BM-EoSs represent the evolution of the unit-cell parameters and the elasticity within the measurement uncertainties, and thus the parameters are at least meaningful in the sense that they represent the measured physical properties of the material.

While it is clear that K-vacancy ordering also affects the intensity and sharpness of the satellite reflections (Foreman and Peacor 1970; McConnell 1981; Merlino 1984), our results show that the subsidiary reflections of nepheline are dependent upon both the displacement of the O1 oxygen from the triad axis, and the long-range ordering of these displacements. The Rigid Unit Mode (RUM) calculations performed by Hayward et al. (2000) on nepheline confirm that the nature of the subsidiary reflections is essentially determined by the framework topology. The role of the extra-framework content is only secondary: their in-situ high-temperature X-ray diffraction and IR-spectroscopy experiments showed that the intensity of the satellite reflections sharply decreases at 308 K for (K,vacancy)-disordered nepheline and 452 K for (K,vacancy)-ordered nepheline.

Our observations of fully reversible changes in the structure of nepheline at high pressures are consistent with the satellite reflections being the result of RUM fluctuations of the tetrahedral framework; the application of pressure decreases the amplitude of the RUM (corresponding to the shift of the O1 toward the triad) without significantly affecting either its coherence or its wavelength. Above ~2 GPa the O1 sits on the triad so the RUM is destroyed and the resulting T1-O1-T2 angle of 180° found in the refined structures at high pressures is thus a true representation of the local structure and not an average of dynamically fluctuating angles as found at high temperatures. The spontaneous reappearance of the satellite intensities upon pressure release, and the fact that the recovered sample displays the same average structure, can only be explained by the framework having an instability corresponding to a specific wave vector, or RUM.

Acknowledgments

G. Diego Gatta thanks the Società Italiana di Mineralogia e Petrologia and the support of NSF grants EAR-0229472 to Nancy Ross and EAR-0408460 to N.L. Ross and R.J. Angel for supporting his research visit to Virginia Tech. The authors thank Jing Zhao (VT) for his help with the experiments. Ruby pressure determinations were conducted with the Raman system in the Vibrational Spectroscopy Laboratory in the Department of Geosciences at Virginia Tech. Ross Angel thanks J. Desmond McConnell for introducing him as an undergraduate to the challenge of incommensurate structures including nepheline, and Michael Carpenter and Tiziana Boffa-Ballaran for more recent discussions.

References cited

Angel, R.J. (2000) Equation of State. In R.M. Hazen and R.T. Downs, Eds., High-Temperature and High-Pressure Crystal Chemistry, 41, p. 35–59. Reviews in Mineralogy and Geochemistry, Mineralogical Society of, Chantilly, Virginia.

——— (2001) EoSFit v6.0.Computer program. Crystallography Laboratory, Department Geological Sciences, Virginia Tech, Blacksburg, www.crystal.vt.edu.

——— (2002) Absorb v5.2. Computer program. Crystallography Laboratory, Department Geological Sciences, Virginia Tech, Blacksburg, www.crystal.vt.edu.

——— (2003a) Automated profile analysis for single-crystal diffraction data. Journal of Applied Crystallography, 36, 295–300.
——— (2003b) WinIntegrStp v3.4. Computer program. Crystallography Laboratory, Department Geological Sciences, Virginia Tech, Blacksburg, www.crystal.vt.edu.
Angel, R.J and Jackson, J.M. (2002) Elasticity and equation of state of orthoenstatite, $MgSiO_3$. American Mineralogist, 87, 558–561.
Angel, R.J., Allan, D.R., Miletich, R., and Finger, L.W. (1997) The use of quartz as an internal pressure standard in high-pressure crystallography. Journal of Applied Crystallography, 30, 461–466.
Angel, R.J., Downs, R.T., and Finger, L.W. (2000) High-Temperature-High-Pressure Diffractometry. In R.M. Hazen and R.T. Downs, Eds., High-Temperature and High-Pressure Crystal Chemistry, 41, p. 559–596. Reviews in Mineralogy and Geochemistry, Mineralogical Society of America, Chantilly, Virginia.
Angel, R.J., Bujak, M., Zhao, J., Gatta, G.D., and Jacobsen, S.D. (2007) Static and ultrasonic observations on the effective hydrostatic limits of pressure media for high-pressure studies. Journal of Applied Crystallography, 40, 26–32.
Baerlocher, C.A. and Meier, W. (1977) DLS-76. A program for the simulation of crystal structures by geometric refinement, http://olivine.ethz.ch/LFK/software/xrs/dls76.html.
Birch, F. (1947) Finite elastic strain of cubic crystal. Physical Review, 71, 809–824.
Bonczar, L.J. and Barsch, G.R. (1975) Elastic and thermoelastic constants of nepheline. Journal of Applied Physics, 46, 4339–4340.
Burnham, C.W. (1966) Computation of absorption corrections and the significance of end effects. American Mineralogist, 51, 159–167.
Dollase, W.A. (1970): Least-squares refinement of the structure of a plutonic nepheline. Zeitschrift fuer Kristallographie, 132, 27–44.
Dollase, W.A. and Peacor, D.R. (1971) Si-Al ordering in nephelines. Contribution to Mineralogy and Petrology, 30, 129–134.
Dollase, W.A. and Thomas, V.M. (1978) The crystal chemistry of silica-rich, alkali-deficient nepheline. Contribution to Mineralogy and Petrology, 66, 311–318.
Foreman, N. and Peacor, D.R. (1970) Refinement of the nepheline structure at several temperatures. Zeitschrift fuer Kristallographie, 132, 45–70.
Gregorkiewitz, M. (1984) Crystal structure and Al/Si-ordering of a synthetic nepheline. Bulletin de Minéralogie, 107, 499–507.
Hahn, T. and Buerger, M.J. (1955) The detailed structure of nepheline, $KNa_3Al_4Si_4O_{16}$. Zeitschrift fuer Kristallographie, 106, 308–338.
Hayward, S.A., Pryde, A.K.A., de Dombal, R.F., Carpenter, M.A., and Dove M.T. (2000) Rigid Unit Modes in disordered nepheline: a study of a displacive incommensurate phase transition. Physics and Chemistry of Minerals, 27, 285–290.
Heinz, D.L. and Jeanloz, R. (1984) The equation of state of the gold calibration standard. Journal of Applied Physics, 55, 885–893.
King, H.E. and Finger, L.W. (1979) Diffracted beam crystal centering and its application to high-pressure crystallography. Journal of Applied Crystallography, 12, 374–378.
McConnell, J.D.C. (1962) Electron-diffraction study of subsidiary maxima of scattered intensity in nepheline. Mineralogical Magazine, 33, 114–124.
——— (1981) Time-temperature study of the intensity of satellite reflections in nepheline. American Mineralogist, 66, 990–996.
Merlino, S. (1984) Feldspathoids: their average and real structures. In W.L. Brown, Ed., Feldspars and feldspathoids. Structures, properties and occurrences, 137, p. 435–470. NATO Advanced Study Institutes, Series C: Mathematical and Physical Sciences, Dordrecht.
Miletich, R., Allan, D.R., and Kuhs, W.F. (2000) High-pressure single-crystal techniques. In R.M. Hazen and R.T. Downs, Eds., High-temperature and high-pressure crystal chemistry, 41, p. 445–519. Reviews in Mineralogy and Geochemistry, Mineralogical Society of America, Chantilly, Virginia.
Oxford Diffraction (2005) Oxford Diffraction Ltd., Xcalibur CCD system, CrysAlis Software system.
Parker, J.M. (1972) The domain structure of nepheline. Zeitschrift fuer Kristallographie, 136, 255–272.
Parker, J.M. and McConnell, J.D.C. (1971) Transformation behaviour in the mineral nepheline. Nature Physical Science, 234, 178–179.
Ralph, R.L. and Finger, L.W. (1982) A computer program for refinement of crystal orientation matrix and lattice constants from diffractometer data with lattice symmetry constraints. Journal of Applied Crystallography, 15, 537–539.
Sahama, T.G. (1958) A complex form of natural nepheline from Iivaa-ra, Finland. American Mineralogist, 43, 165–166.
——— (1962) Order–disorder in natural nepheline solid solutions. Journal of Petrology, 65–81.
Sheldrick, G.M. (1997) SHELX-97. Programs for crystal structure determination and refinement. University of Göttingen, Germany.
Simmons, W.B., Jr. and Peacor, D.R. (1972) Refinement of the crystal structure of a volcanic nepheline. American Mineralogist, 57, 1711–1719.
Stebbins, J.F., Murdoch, J.B., Carmichael, I.S.E., and Pines, A. (1986) Defects and short-range order in nepheline group minerals: a silicon-29 nuclear magnetic resonance study. Physics and Chemistry of Minerals, 13, 371–381.
Tait, K.T., Sokolova, E., and Hawthorne, F.C. (2003) The crystal chemistry of nepheline. Canadian Mineralogist, 41, 61–70.
Tilley, C.E. (1954) Nepheline-alkali feldspar paragenesis. American Journal of Science, 252, 62–75.
Wilson, A.J.C. and Prince, E., Eds. (1999) International tables for X-ray crystallography, Volume C: Mathematical, physical and chemical tables (2nd Edition). Kluwer Academic, Dordrecht.

Manuscript received November 7, 2006
Manuscript accepted March 21, 2007
Manuscript handled by Przemyslaw Dera